ACS OMEGA

Open Access

This article is licensed under CC-BY-NC-ND 4.0

http://pubs.acs.org/journal/acsodf

Article

Carbon Dot Nanozyme Ameliorating Ischemia-Reperfusion-Induced Muscle Injury by Antioxidation and Downregulating iNOS/COX-2 Pathway

Wenbin Fan,[▽] Qing-Ying Luo,[▽] Xun Lu, Qing Xie, Qunzeng Danzeng, Yiqian Zhang, Song Jin,* Wen-Xiang Cheng,* and Cui Liu*

Cite This: *ACS Omega* 2024, 9, 28666−28675

Read Online

ACCESS | Metrics & More | Article Recommendations | Supporting Information

ABSTRACT: Skeletal muscle ischemia-reperfusion (IR) injury is a prevalent type of muscle injury caused by events, such as trauma, arterial embolism, and primary thrombosis. The development of an IR injury is associated with oxidative stress and an excessive inflammatory response. Nanozymes, which have exceptional free radical scavenging activities, have gained significant attention for treating oxidative stress. This study demonstrates that carbon dot (C-dot) nanozymes possess superoxide dismutase (SOD)-like activity and can act as free radical scavengers. The carbon dot nanozymes are presented to mitigate inflammation by downregulating the iNOS/COX-2 pathway and scavenging reactive oxygen−nitrogen species to reduce oxidative stress, thereby suppressing inflammation. In the IR injury of skeletal muscle mice, we demonstrate that C-dots can effectively reduce inflammatory cytokines and tissue edema in skeletal muscle following IR injury in the limb. These findings suggest that C-dots have potential as a therapeutic approach for IR injury of skeletal muscle with negligible systemic toxicity. This offers a promising strategy for clinical intervention.

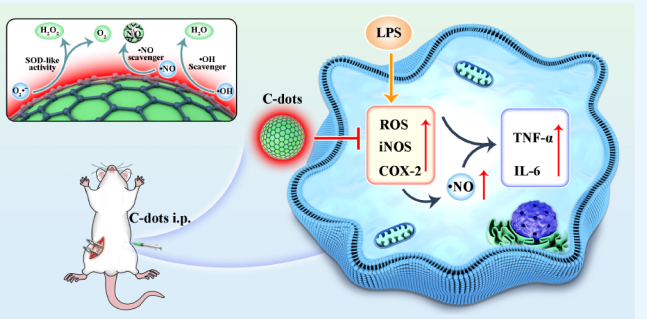

INTRODUCTION

Skeletal muscle ischemia-reperfusion (IR) injury is a prevalent clinical muscle injury, which caused by various factors such as trauma, arterial embolism, primary thrombosis, arterial grafting, amputation and replantation, fascial interval syndrome, and prolonged application of tourniquet.[1,2] It is not limited to localized skeletal muscle tissues but can trigger systemic inflammatory response syndrome and lead to functional damage in multiple organs. Various strategies, including physical and chemical treatments, have been used to treat limb IR injury. Regrettably, there are currently no effective treatments available for this situation.[3] A crucial factor in reperfusion injury is the dysfunction of capillary microcirculation triggered by oxidative stress and inflammatory response, which subsequently results in the phenomenon of capillary no-reflow, ultimately leading to cell death (necrosis and/or apoptosis).[4] Therefore, antioxidant and anti-inflammatory therapies hold significant promise as treatments for IR injury. For example, restoring perfusion to ischemic skeletal muscle with blood enriched with oxygen radical scavengers, such as superoxide dismutase (SOD), catalase, and glutathion peroxidase, effectively attenuated reperfusion injury.[5] In addition, hypothermia,[6] light diode therapy,[7] dexamethasone,[8] silibinin,[9] hydrogen-rich saline[10] have been reported to attenuate severe skeletal damage induced by limb IR injury. Despite the success of the above procedures and drugs in the laboratory, none of them are proven effective in clinical settings. Consequently, it is urgent to seek new agents with multiple properties to treat IR injury.

Nanomedicine promises to implement site-specific treatment compared to the administration of free agents, which has obvious advantages in terms of stability, drug loading efficiency, pharmacokinetics, targeting ability, safety, and multifunctionality. As the mainstay of nanomedicine, delivering therapeutics to maximize efficacy and minimize off-target toxicity can be realized through overcoming pathophysiological obstacles.[11,12] The extensive body of research on nanozymes, encompassing hundreds of nanomaterials comprising metals and metal oxides and their various compositions, indicates that they exhibit catalytic activity comparable to that of natural enzymes. Nanozymes, which comprise iron oxide, gold, carbon-based materials, and other materials, are related to

Received: March 25, 2024
Revised: May 28, 2024
Accepted: May 29, 2024
Published: June 20, 2024

© 2024 The Authors. Published by American Chemical Society

Scheme 1. Schematic Illustration of C-dot Nanozyme Ameliorating IR-Induced Muscle Injury by Antioxidation and Downregulating iNOS/COX-2 Pathway

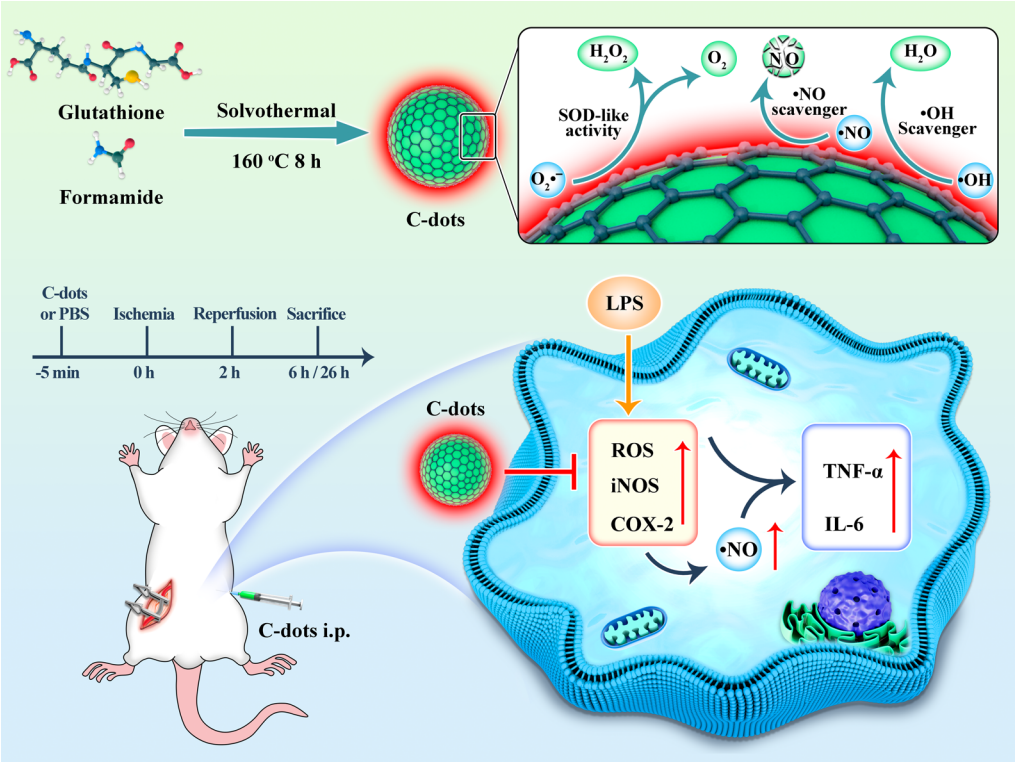

their intrinsic enzyme-mimetic activities.[13−15] Compared with natural enzymes, nanozymes have advantages such as low cost, high stability, and durability, which have been widely used in industrial, medical, and biological fields. C-dots, a new class of zero-dimensional nanomaterials, have received extensive research attention due to their unique fluorescence properties, biocompatibility, cost-effectiveness, and ease of functionalization.[15−17] In addition, C-dots, which are one of the nanozyme based on carbon nanomaterials, exhibit good enzyme-like catalytic activity due to their small particle size (usually less than 5 nm), large specific surface area, and high reactivity, making them excellent electron donors and electron acceptors.[18,19] C-dots with antioxidant enzyme activity, which can scavenge reactive oxygen species (ROS), have been used in the treatments of cerebral IR injury,[20] acute lung injury,[21] colitis,[22,23] acute liver injury,[24] diabetic wounds,[25,26] and have achieved remarkable therapeutic effects. It is well-known that IR injury is chronologically divided into two phases: ischemia following blood supply interruption and reperfusion upon blood supply resoration,[27] with the duration of ischemia playing a crucial role in determining reperfusion injury. Compare to other tissue units, skeletal muscle is more vulnerable to IR injury, with a tolerance limit of only 4 h, significantly lower than that of skin, peripheral nerves, and bone.[28] However, it remains unknown whether C-dot nanozymes can protect against skeletal muscle IR injury.

Fluorescent C-dots nanozyme with SOD-like activity was generated by a solvothermal method in this study. This C-dot SOD nanozyme showed good fluorescence and remarkable SOD-like activity, which can not only scavenge the source of ROS, i.e., superoxide anion, but also scavenge hydroxyl radicals, nitric oxide radicals, and singlet oxygen. In addition, the C-dots can downregulate the expression level of inducible nitric oxide synthase (iNOS) and cyclooxygenase-2 (COX-2) through the activation of transcription factor NF-E2-related factor 2 (Nrf2) and a KELCH-like ECH-associated protein 1 (Keap1)-mediated ubiquitination pathway. The synergistic effect makes C-dots have a significant therapeutic effect on skeletal muscle IR injury. These findings highlight the multitasking capabilities of C-dot nanozymes, such as antioxidant, anti-inflammatory, and regulators of gene expression, making them promising candidates for the treatment of IR-related diseases (Scheme 1).

MATERIALS AND METHODS

Synthesis. Synthesis of C-dots: 2.1 g of glutathione was added into 70 mL of formamide and reacted in an autoclave at 160 °C for 8 h.[29−31] To exclude any precipitates, the resulting solution was centrifuged at 3000 rpm for 10 min after the reaction. The solution was dialyzed for 5−7 days by using a 3500 Da dialysis bag. For further purification, the C-dot solution was frozen at −20 °C for 6 h and then thawed at room temperature. To remove the precipitate by filtration, the thawed solution was centrifuged at 12 000 rpm for 10 min. This process was typically repeated 4−5 times. Finally, the powder of C-dots was obtained by vacuum freeze-drying from the resulting supernatant.

Measurement of Electron Spin Resonance (ESR). The ESR signal of the free radical spin adduct was utilized to quantitatively estimate the free radicals, determining the peak-to-peak height of the ESR spectrum. To scavenge superoxide anion, 50 μL of graphite-like carbon nitride ($g\text{-}C_3N_4$) solution (0.5 mg/mL in methanol) was mixed with 10 μL of 5,5-dimethyl-1-pyrroline N-oxide (DMPO) and 40 μL of pure methanol or C-dots (in methanol, at final concentrations of 20,

https://doi.org/10.1021/acsomega.4c02869
ACS Omega 2024, 9, 28666−28675

50, 100 μg/mL). Then, the mixture was exposed to a 300 W xenon lamp for 5 min before ESR measurements.

For hydroxyl radical scavenging, 10 μL of DMPO and 80 μL of pure water or C-dots (at final concentrations of 20, 50, and 100 μg/mL in water) were added to a 100 μL $FeSO_4$ solution (5 mg/mL in water). The mixture was then supplemented with 10 μL of H_2O_2 (30%) and stirred at room temperature for 5 min before the ESR measurement.

For nitric oxide-free radical scavenging, 20 μL of *N*-[3-[1-[[4-(3,4-difluorophenoxy) phenyl] methyl]-4-piperidinyl]-4-methylphenyl]-2-methylpropanamidehydrochloride (SNAP) solution (in 40 mM PBS, pH7.4), 20 μL of 2-(4-carboxyphenyl)-4,4,5,5-tetramethylimidazoline-1-oxyl-3-oxide potassium salt (Carboxy-PTIO) solution, and 20 μL of PBS solution or C-dot solution (100 μg/mL in PBS) were mixed and reacted for 10 min before ESR measurements.

For singlet oxygen scavenging, 50 μL of aqueous solution of titanium oxide (TiO_2) nano powder (2 mg/mL), 50 μL of 2,2,6,6-tetramethylpiperidine (TEMP) solution (100 mM), and 100 μL of pure water or C-dots (100 μg/mL in water) were mixed thoroughly. The mixture was performed in a capillary tube and then illuminated with a 300 W xenon lamp for 10 min before ESR measurements.

SOD Enzyme Activity Assay. The activity of the SOD enzyme was evaluated with the Total Superoxide Dismutase Assay Kit. The test was performed following vendor's indications to measure the SOD-like activity of C-dots at various concentrations as the inhibitory rate of the WST-1 reaction. The plate reader recorded the absorbance at 450 nm.

Cytotoxicity Assay. The cytotoxicity of the C-dots was tested in three different cell lines, RAW264.7, A549, and EA.hy926 cells (ATCC, USA) by cell counting kit-8 (CCK-8) assay. Cells were placed in 96-well plates at a density of 3×10^3 cells per well and cultured for 24 h. Subsequently, they were treated with C-dots at the indicated concentrations for 24 h. The measurement of the absorbance at 450 nm was taken.

Flow Cytometry Analysis of Intracellular C-Dots. The amount of C-dots accumulated in RAW264.7 cells was measured by flow cytometry using a Beckman CytoFLEX S device. Cells were seeded in a 6-well plate and given 50 μg/mL C-dots for variable time periods. These included 0, 5, 10, 20, 30, and 60 min. Afterward, the cells were gently removed from the plate, collected, and rinsed with PBS. The cells were resuspended (approximately 5×10^5 cells) in 400 μL of PBS. The APC-A channel was used to measure fluorescence intensity. Flow cytometry data were analyzed using Flow Jo software.

Confocal Laser Scanning Fluorescence Microscopy. RAW264.7 cells were seeded on glass coverslips and treated with 100 μg/mL C-dots for 24 h. The coverslip was rinsed with PBS and mitochondria, and lysosomes were stained using a fluorescence probe. The samples were fixed with 4% paraformaldehyde for 20 min and then dyed with 4′,6-diamidino-2-phenylindole (DAPI) for 3 min at normal room temperature. The cells were observed by using a confocal laser scanning fluorescence microscope.

Enzyme-Linked Immunosorbent Assay (ELISA). C-dots were cocultured with RAW264.7 cells at the indicated concentrations for 2 h, followed by exposure to 50 ng/mL lipopolysaccharides (LPS) for 24 h. The concentrations of interleukin-6 (IL-6) and tumor necrosis factor-alpha (TNF-α) in the supernatant were detected by commercially available ELISA kits. The cytokine concentrations were calculated using the standard curve generated according to the instructions.

Scavenges Intracellular ROS in RAW264.7 Cells. Intracellular ROS accumulation was monitored using the fluorescent probe DCFH-DA. RAW264.7 cells were seeded in a 96-well plate. Cells were stimulated with 100 ng/mL LPS for 90 min after pretreatment with a specific concentration of C-dots for 3 h. Subsequently, the cells were incubated at 37 °C for 30 min avoiding light, followed by washing with Hank's balanced salt solution (HBSS). The samples were observed under a fluorescence microscope with a 488 nm excitation and 530 nm emission.

Immunoblotting. RAW 264.7 cells were pretreated for 2 h using C-dots and then exposed to LPS (100 ng/mL) for 24 h. The cells were lysed using RIPA lysis buffer and subjected to Western blot analysis. Each sample's protein (50 μg) was electrophoretically separated by SDS-PAGE and then transferred to a polyvinylidene fluoride membrane. After blocking with 5% skim milk powder, the membrane was then incubated with antibodies specific for iNOS, COX-2, Keap1, Nrf2, and GAPDH at 4 °C during the night, followed by secondary antibody incubation.

Nitric Oxide (NO) Detection. We used the Griess reaction to determine the nitrite concentration in the culture medium to indicate NO production. The RAW264.7 cells were preincubated with C-dots at concentrations of 0, 7.5, 15, 30, and 60 μg/mL and then subsequently stimulated with 100 ng/mL LPS. The nitrite levels were measured by following the manufacturer's recommendations and measuring the absorbances at 540 nm. Calculate the standard curve to determine the concentrations of sodium nitrite.

Animal and Treatment. Male C57BL/6 mice aged 8−10 weeks were housed in specific pathogen-free animal research facilities, obtained from GemPharmatech in Foshan, China. The mice were randomly divided into five groups, including control and model, treated, or not treated with C-dots at two time points. IR injury mice were established by blocking the femoral artery and vein using the microvascular clamp for 2 h. Then, the clamp was removed to induce reperfusion. The whole blood and skeletal muscle samples were collected after 4 and 24 h after reperfusion. The mice in the C-dots group were given an intraperitoneal injection (ip) of 50 mg/kg prior to IR injuries. The Institutional Animal Care and Usage Committee of the Shenzhen Institutes of Advanced Technology (SIAT-IACUC-190723-KYC-ZP-A0804) approved all animal protocols.

Histology. To assess general histology, sections of muscle (4 μm) were stained with H&E. Muscle sections (4 μm) were stained with H&E. Two independent pathologists assessed limb muscle damage by calculating the extent of damage in three randomly selected fields. Healthy fibers were identified as having complete, regularly arranged borders without punctures, fractures, or edema. Injured fibers were associated with edema, which resulted in the fibers being broken and fragmented.

The biocompatibility of the C-dots was evaluated by administering them continuously to mice over a period of 30 days. Tissue samples from the five major organs were harvested, including the heart, liver, spleen, lungs, and kidneys. The tissue sample was fixed in 10% formalin, embedded in paraffin, and then sliced into 4 μm-thick slices. The slices were deparaffinized and stained with hematoxylin and eosin. Microscope equipped with a 10× magnifying lens was used.

https://doi.org/10.1021/acsomega.4c02869
ACS Omega 2024, 9, 28666−28675

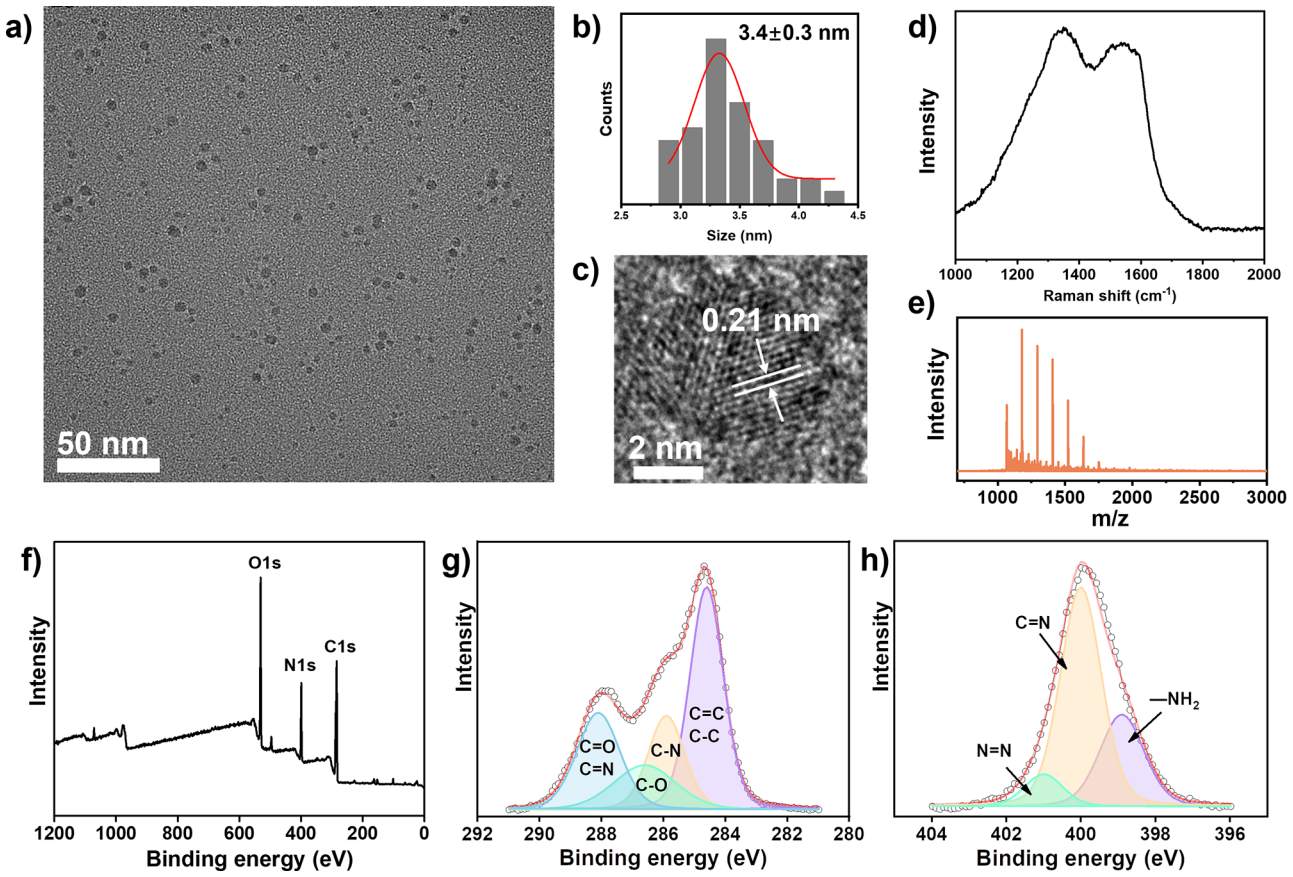

Figure 1. TEM image (a), statistical size distribution obtained from TEM (b), high-resolution TEM image (c), Raman spectrum (d), molecular weight distribution from MALDI-TOF (e), XPS survey (f), and high resolution XPS of C 1s (g) and N 1s (h) with peaks identified by curve fitting of C-dots.

Hematology Analysis and Hepatorenal Functions Assessment. Whole blood from mice was collected at the end point of the study. The blood samples were divided into two portions. Whole blood sample for routine blood was analyzed using an Auto Hematology Analyzer. Serum was separated for liver and kidney function tests by the Automated Chemistry Analyzer System. A total of five indicators were the subject of testing, among which were alanine transaminase (ALT), aspartate aminotransferase (AST), alkaline phosphatase (ALP), creatinine (CREA) and blood urea nitrogen (BUN) measurements.

In Vivo Tracking of C-Dots. C-dots (5 mg/kg) in PBS were administered intraperitoneally to male C57BL/6 mice. As a negative control, an equal amount of PBS was administered. Tissues from the heart, liver, spleen, lungs, and kidneys were harvested at 0.5, 1, 2, 6, and 24 h after treatment. The accumulation of C-dots was determined using the *in vivo* imaging system.

RESULTS AND DISCUSSION

Synthesis and Characterization of C-Dots. C-dot SOD nanozymes that have red fluorescence were obtained using a solvothermal method by reacting glutathione with formamide at 160 °C for 8 h.[29−31] The resulting nanomaterials were purified by filtration, dialysis, and repeated freeze−thawing. The transmission electron microscopy (TEM) image (Figure 1a) showed that the C-dots present monodisperse with a statistical average particle size of about 3.4 nm (Figure 1b) and a lattice spacing of graphite 100 of 0.21 nm (Figure 1c). The Raman spectrum of C-dots showed two scattering peaks at 1350 and 1590 cm^{-1} (Figure 1d), which correspond to the D and G bands of graphene, respectively, implying a large number of defective structures within C-dots. The ^{1}H NMR spectrum of C-dots is shown in Figure S1, which reveals peaks at 1−1.8 and 7.5−8.5 ppm, indicating the presence of saturated carbon−hydrogen bonds and aromatic hydrocarbons, respectively, on C-dots. The peaks in the range of 3.0−4.5 ppm implied the existence of hydroxyl, carbonyl or amino groups on the C-dot surface. MALDI-TOF was used to determine the molecular weight of the C-dot nanozyme, and the result showed that the molecular weight distribution of the C-dots was in the range of 1000−1800 Da, with an average particle size of about 1300 Da (Figure 1e). Fourier transform infrared (FT-IR) spectra confirmed the presence of abundant hydroxyl and amino groups (3150−3350 cm^{-1}) on the C-dot surface, along with amide bonds (1678 cm^{-1}) and C═C (1600 cm^{-1}). The absorption at 1396 cm^{-1} could be attributed to C−N stretching vibration or an O−H in-plane bending vibration (Figure S2).[21,21] In addition, X-ray photoelectron spectroscopy (XPS) was employed to analyze the structure of the C-dots, which revealed that the C-dots mainly consisted of four elements, C, N, O, and S, in the ratio of 59.14:16.78:22.64:1.45 (Figure 1f). The high-resolution C 1s spectrum (Figure 1g) was fitted with four peaks located at 284.6, 285.9, 286.6, and 288.1 eV, which were attributed to C═C/C−C, C−N, C−O, and C═N/C═O, respectively. The high-resolution N 1s spectrum (Figure 1h) was fitted with three peaks located at 398.9, 400.0, and 401.0 eV, attributing to amino N−H, C═N,

https://doi.org/10.1021/acsomega.4c02869
ACS Omega 2024, 9, 28666−28675

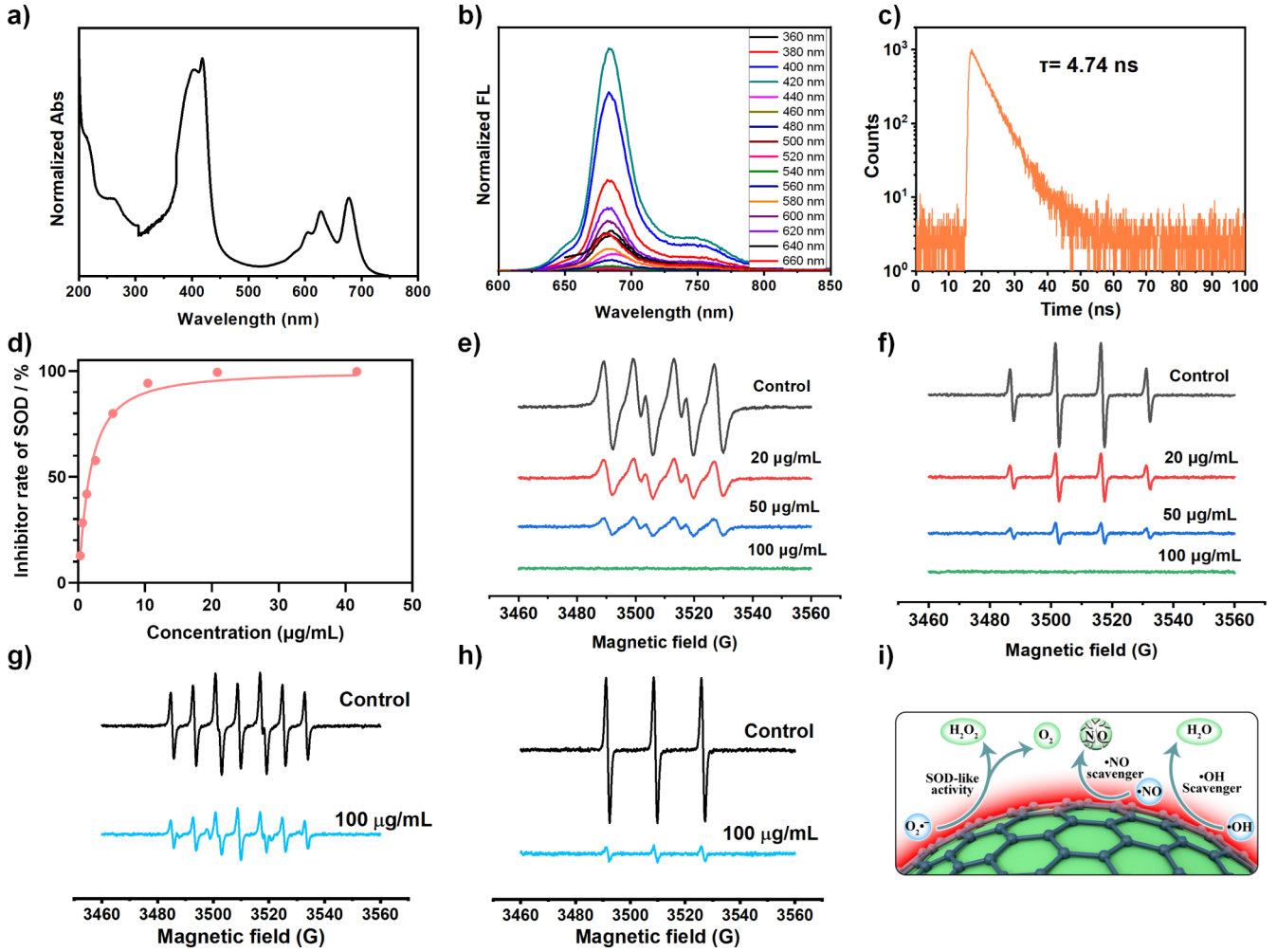

Figure 2. UV−vis absorption (a) and fluorescence emission (b) spectra of C-dots; time-resolved fluorescence curve of C-dots under excitation and emission wavelengths of 405 and 680 nm, respectively (c); the SOD-like activity of C-dots (d), O_2•$^-$ (e), •OH (f), •NO (g), and singlet oxygen (h) scavenging activities of C-dot; schematic presentation of broad-spectrum antioxidant activity of C-dots (i).

and N═N, respectively. The high-resolution O 1s spectrum (Figure S3) exhibited two peaks centered at 531.5 and 533.0 eV after fitting, which can be assigned to C═O and C−O, respectively[29]. These results indicated that the C-dots were composed of N-doped graphite with abundant oxygen- and nitrogen-containing functional groups on the surface or edges.

Fluorescence and Antioxidant Enzyme-Like Activity of C-Dots. Subsequently, the fluorescence and catalytic properties of the C-dots were investigated. The UV−vis absorption and emission spectra of C-dots are shown in Figure 2a,b. The C-dot absorption spectrum (Figure 2a) displayed strong absorption in the ranges of 400−420 nm and 600−670 nm, corresponding to the $\pi \rightarrow \pi^*$ and n $\rightarrow \pi^*$ transitions, respectively.[29] The optimal emission wavelength of this C-dots was 680 nm (Figure 2b), and the absolute fluorescence quantum yield (QY) was determined to be 23% using an integrating sphere system, which was significantly higher than the previously reported result of 16.8%.[29] This enhancement in QY was probably due to the repeated freezing and thawing processes, ultimately enhancing the stability of C-dots. The fluorescence lifetime of the C-dots is 4.74 ns (Figure 2c), exhibiting a monoexponential decay profile, which confirms a single excited state decay pathway of C-dots, suggesting that the excited C-dots back to the ground state mainly through the radiative fluorescence pathway.[32] The SOD-like activity of C-dots was evaluated by a commercialized kit (Figure 2d). Remarkably, when the C-dot concentration reached 10 μg/mL, the removal rate of the superoxide anion exceeded 90%, indicating the high SOD enzyme activity of these C-dots. In addition, ESR results demonstrated the scavenging ability of these C-dots to scavenge O_2•$^-$ (Figure 2e), •OH (Figure 2f), •NO (Figure 2g), and singlet oxygen (Figure 2h). The SOD-like activity of C-dots has been studied in complex environments to investigate the effects of various regular molecules, such as BSA, leucine, glutathione, lysine, glucose, histidine, ascorbic acid, and phenylalanine. As shown in Figure S4, no significant influence of these molecules on the SOD-like activity of C-dots was observed. This proved the potential applications to scavenge various reactive species in a complex environment. These results illustrated the potential of these C-dot SOD nanozymes for applications in both bioimaging and antioxidant.

Antioxidative Stress and Anti-Inflammatory Properties of C-Dots In Vitro. Next, the capability of C-dot nanozymes to penetrate living cells was investigated. The intracellular fluorescence was used to monitor the uptake of C-dot nanozymes by living cells due to their good fluorescence properties.[21] As shown in Figures 3a and S5, the fluorescence

https://doi.org/10.1021/acsomega.4c02869
ACS Omega 2024, 9, 28666−28675

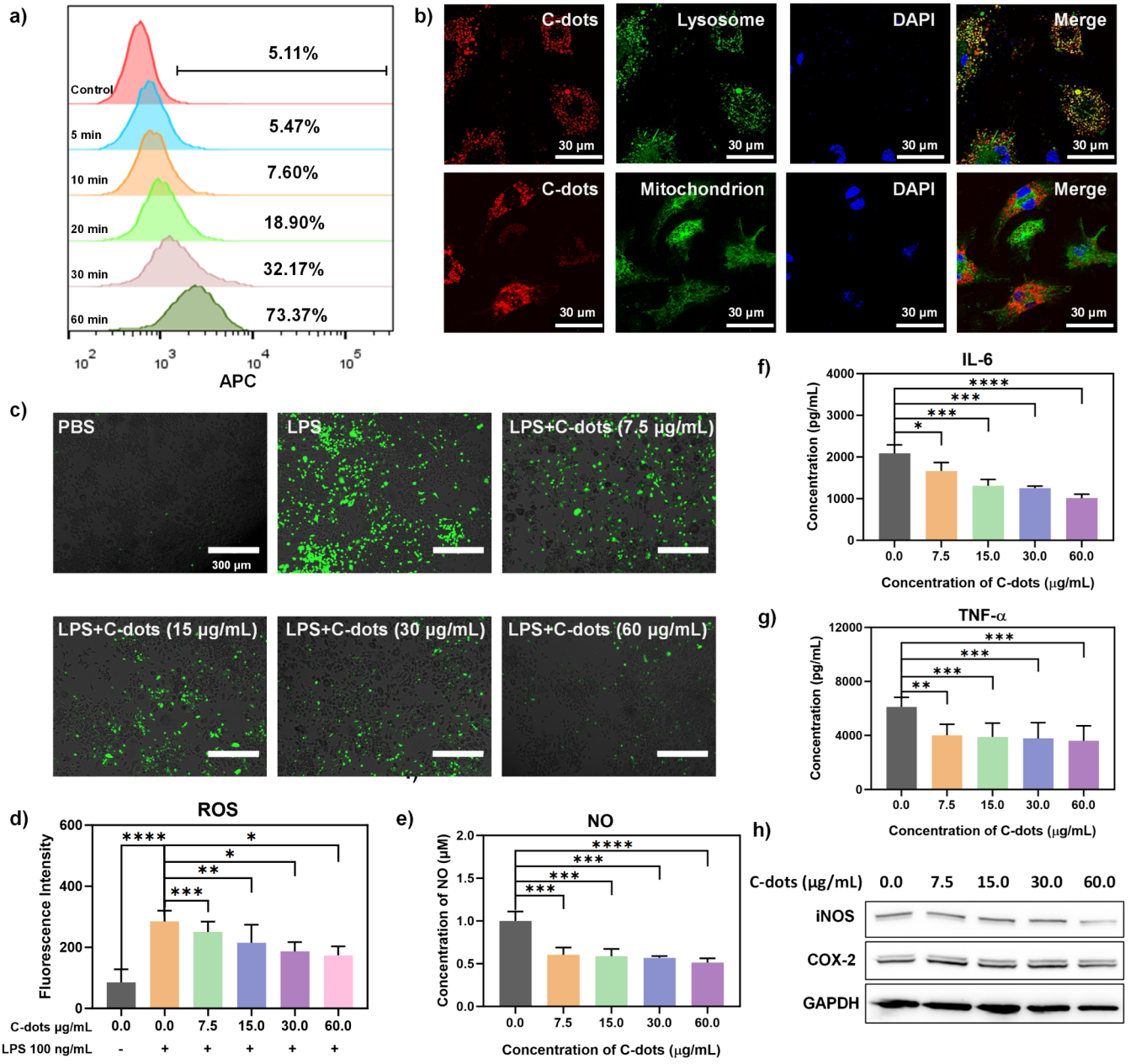

Figure 3. Flow cytometry results of C-dot accumulation in Raw264.7 cells under various incubation time (a). Colocalization images of C-dots with lysosome (b, upper) or mitochondria (b, bottom), ROS staining by fluorescent probe of DCFH-DA in Raw264.7 cells under different concentrations of C-dot treatments (c), the variation of FL intensity of fluorescence probe of DCFH-DA in Raw264.7 cells under various treatment conditions (d), the concentration variation of NO in LPS-treated Raw264.7 cells with pretreated with C-dots (e), ELISA assay of IL-6 (f) and TNF-α (g) after different treatments of the Raw264.7 cells. Western blot images of COX-2 and iNOS expressions in Raw264.7 cells stimulated by LPS under various treatment conditions (h).

from intracellular C-dots became detectable after 10 min of coincubation with Raw264.7 cells and reached peak intensity after 1 h. By organelle staining, we found that C-dots were mainly enriched in lysosomes after cellular uptake, indicating that these C-dots might enter living cells through endocytosis (Figure 3b). Moreover, when coincubated with the C-dot for 24 h, three kinds of cell lines, including Raw264.7, A549, and EA.hy926, retained good cell viability (Figure S6), indicating the good biocompatibility of C-dots. In previous reports, modification of nanoparticles helps them not only avoid clearance by macrophages but also suppresses their internalization by target cells. The entire surface structure and geometry play a significant role, rather than relying on a single factor such as maximizing repulsion force through polymer-based steric stabilization (e.g., PEGylation) or inhibiting immune attack through a bioinspired component.[33] Consequently, in the subsequent research, we aim to optimize surface modification to the surface of nanoparticles in order to facilitate their capture by target cells *in vivo*.

To induce an inflammatory response and increase intracellular ROS levels, LPS was utilized. Figures 3c,3d, and S7 showed that the green fluorescence of the cells decreased in the group pretreated with C-dot nanozymes, indicating that these C-dot nanozymes could effectively remove the intra-

https://doi.org/10.1021/acsomega.4c02869
ACS Omega 2024, 9, 28666−28675

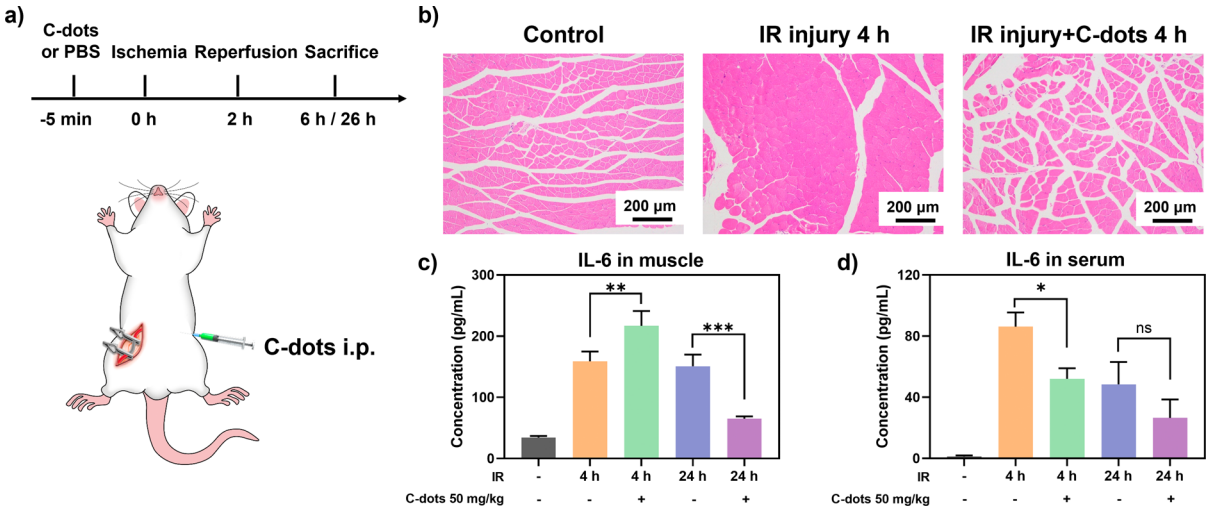

Figure 4. Illustration of study design (a), H&E staining of muscle tissue (b), IL-6 expression level in muscle tissue (c) and serum (d).

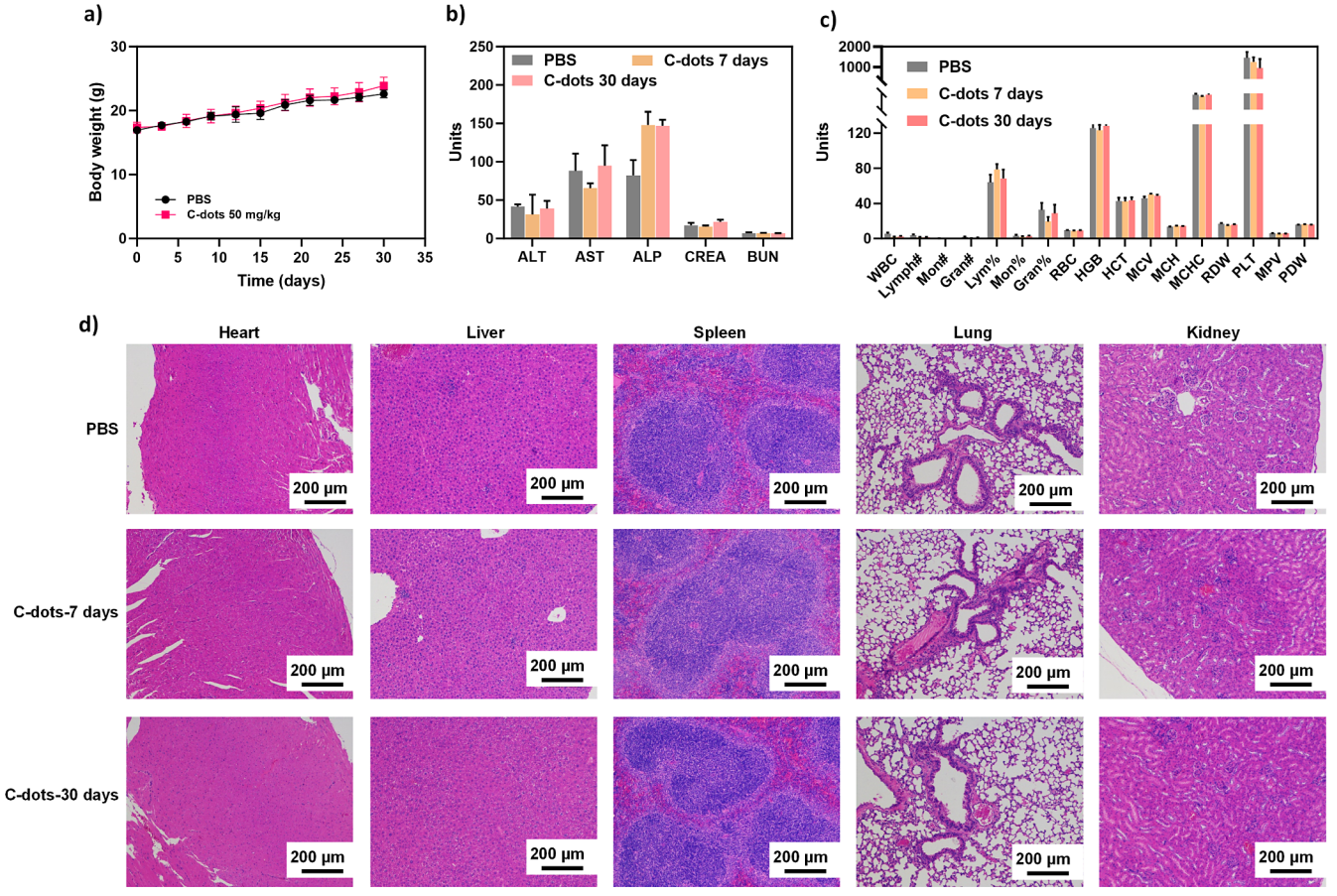

Figure 5. Biocompatibility of C-dots was evaluated through body weight change of mice with and without injection of C-dots (a), blood biochemical analysis (b), and routine blood analysis (c). Additionally, H&E staining was performed on the heart, liver, spleen, lungs, and kidneys of mice with and without injection of C-dots (d).

cellular ROS to maintain the intracellular redox balance. Additionally, the content of NO, which can be scavenged by C-dot nanozymes, was measured in LPS-treated cells with pretreatment of C-dots (concentration from 0 to 60 μg/mL). As shown in Figure 3e, the content of NO in living cells pretreated with C-dot nanozymes was reduced. TNF-α and IL-6 are common inflammatory factors, and their expression levels reflecting the initiation and progression of inflammation.[20] As shown in Figure 3f,3g, pretreatment with C-dot nanozymes resulted in a significant decrease of inflammatory factors in LPS-treated cells, suggesting that C-dot nanozymes have significant anti-inflammatory effects by scavenging ROS and reactive nitrogen species (RNS) and ROS. Furthermore, the expression of iNOS and COX-2 was assessed (Figures 3h and S8), revealing a decrease in their expression following C-dot nanozyme pretreatment. ROS detoxifying enzymes are

https://doi.org/10.1021/acsomega.4c02869
ACS Omega 2024, 9, 28666−28675

predominantly driven by the transcription factor Nrf2, which is tightly regulated by Keap1-mediated ubiquitination.[34,35] The expression of Keap1 and Nrf2 was then analyzed using WB after pretreating with C-dot nanozyme. The results showed that Keap1 expression decreased and Nrf2 expression increased after C-dot nanozyme pretreatment (Figures S9 and S10). The findings indicated that C-dots were capable of reducing the levels of intracellular ROS and RNS and of activating Nrf2/Keap1, in conjunction with regulation of the downstream iNOS/ROS antioxidant signaling pathway. Ultimately, this resulted in antioxidant and anti-inflammatory effects.

Protective Effects of C-Dots on Skeletal Muscle IR Injury and Biocompatibility. To assess the therapeutic potential of the C-dot nanozyme in skeletal muscle IR injurie, a mice model of IR injury was established, and IR injury mice were established by blocking the femoral artery and vein using the microvascular clamp for 2 h. Then, the clamp was removed to induce reperfusion (Figure 4a). Mice in the C-dot nanozyme group were administrated (i.p.) at the dosage of 50 mg/kg prior to IR injuries. C-dots were delivered to the muscles of the hind limb via injection prior to IR injury. The subsequent blockade of blood flow allowed the C-dots to remain in situ within the local tissue, until the tissue was reperfused. This approach resulted in C-dots being accumulated at sites of IR injury. Due to the inflammation plays a significant role in IR,[36] we aimed to investigate the potential of C-dot nanozyme in reducing inflammation levels and tissue edema in skeletal muscle following limb IR injury. Muscle tissue injury was assessed using H&E staining as shown in Figure 4b and S11. The identification of healthy muscle fibers is based on the presence of complete borders that are regularly arranged without any breaks, holes, or edema. In contrast, degeneration of muscle fibers, dissolution of the sarcoplasm, infiltration of inflammatory cells, and myoedema were observed in the IR group, indicating the success of the IR model. While, such conditions were minimal in the C-dot nanozyme treatment group, demonstrating a reduction in inflammation levels of IR mice muscle tissues. As shown in Figure 4c, level of IL-6 was remarkably higher in the IR group compared to the control group, while C-dot nanozyme treatment decreased the level of IL-6 at 24 h after reperfusion. As mentioned above, skeletal muscle IR injury would trigger a systemic inflammatory response, which can be reflected by the level of IL-6 in serum. As shown in Figure 4d, C-dot nanozyme treatment in IR mice alleviated evidently the increments in the serum cytokine level at both 4 and 24 h after reperfusion, indicating C-dot nanozymes could inhibit systemic inflammatory response trigged by skeletal muscle IR injury. It has been reported that NO, produced by iNOS, enhances the activity of COX-2[37] and both contribute to inflammation and progression of IR injury. Combining the in vivo data, we can infer that C-dots may preserve skeletal muscle against limb IR injury through downregulating the iNOS/COX-2 pathway and activating Nrf2/Keap1, reducing oxidative stress, thereby suppressing inflammation.

Evaluation of the Biocompatibility of C-Dots. Numerous studies have consistently shown the remarkable biocompatibility of C-dots. In mice, the cumulative amount of C-dots declined quickly, indicating that C-dots were readily metabolized (Figure S12). Furthermore, as shown in Figure 5a, the change in body weight was similar between the C-dot and non-C-dot groups. Hepatorenal function was assessed by measuring the levels of ALT, AST, ALP, CREA, and BUN, as displayed in Figure 5b. The levels of these indicators in mice at 7 and 30 days after C-dot injection were normal, indicating that C-dots did not result in kidney or liver toxicity. Furthermore, all three groups, including the PBS group and the 7- and 30-day C-dot treatment groups, exhibited normal results in routine blood tests (Figure 5c). Additionally, H&E staining was performed on the heart, liver, spleen, lungs, and kidneys of mice at 7 and 30 day after C-dot injection. The results showed no signs of damage (Figure 5d). These comprehensive findings illustrate the excellent biocompatibility of C-dots when administered at therapeutic doses in mice.

CONCLUSIONS

In summary, we successfully developed a C-dot SOD nanozyme exhibiting remarkable fluorescence properties and exceptional scavenging capability against reactive nitrogen/oxygen species. In vitro experiments demonstrated the C-dots effectively downregulate the iNOS/COX-2 pathway and activate Nrf2/Keap1 patway, thereby inhibiting the generation of ROS and RNS and mitigating excessive inflammation responses. By employing a mice model of IR injury and administering C-dot treatment, we demonstrated significant reductions in inflammation and tissue edema in skeletal muscle following IR injury in the limb. This finding highlights the potential of C-dot nanozyme as a therapeutic drug for mitigating IR injury by targeting the underlying mechanisms of oxidative stress and inflammatory responses.

ASSOCIATED CONTENT

Supporting Information

The Supporting Information is available free of charge at https://pubs.acs.org/doi/10.1021/acsomega.4c02869.

Chemicals and reagents, instrumentation, ^{1}H NMR spectrum of C-dots, FT-IR spectrum of C-dots, high resolution XPS of O 1s of C-dots with identification of peaks by curve fitting, the flow cytometry results of C-dots accumulation in Raw264.7 cells, the viabilities of Raw264.7, A549, and EA.hy926 cells after incubated with C-dots, H&E staining of muscle tissue after 24 h reperfusion, and the distribution of C-dot nanozyme in major organs of healthy mice (PDF)

AUTHOR INFORMATION

Corresponding Authors

Song Jin − *The Eighth Affiliated Hospital of Sun Yat-sen University, Shenzhen 518033, PR China*; Email: jingso@163.com

Wen-Xiang Cheng − *Centre for Translational Medicine Research & Development, Shenzhen Institutes of Advanced Technology, Chinese Academy of Sciences, Shenzhen 518055, PR China*; Email: wx.cheng@siat.ac.cn

Cui Liu − *Chongqing Key Laboratory of Natural Product Synthesis and Drug Research, Innovative Drug Research Center, School of Pharmaceutical Sciences, Chongqing University, Chongqing 400044, PR China*; orcid.org/0000-0002-8399-5765; Email: liucui@cqu.edu.cn

Authors

Wenbin Fan − *The Eighth Affiliated Hospital of Sun Yat-sen University, Shenzhen 518033, PR China; Department of Thoracic Surgery, Huazhong University of Science and*

https://doi.org/10.1021/acsomega.4c02869
ACS Omega 2024, 9, 28666−28675

Technology Union Shenzhen Hospital, Shenzhen 518052, PR China

Qing-Ying Luo − *School of Food and Drug, Shenzhen Polytechnic University, Shenzhen 518055, PR China*

Xun Lu − *Southern medical university The First Clinical Medical School (Nanfang Hospital), Guangzhou 510515, PR China*

Qing Xie − *Chongqing Key Laboratory of Natural Product Synthesis and Drug Research, Innovative Drug Research Center, School of Pharmaceutical Sciences, Chongqing University, Chongqing 400044, PR China*

Qunzeng Danzeng − *Chongqing Key Laboratory of Natural Product Synthesis and Drug Research, Innovative Drug Research Center, School of Pharmaceutical Sciences, Chongqing University, Chongqing 400044, PR China*

Yiqian Zhang − *The Eighth Affiliated Hospital of Sun Yat-sen University, Shenzhen 518033, PR China;* orcid.org/0000-0002-8904-7424

Complete contact information is available at: https://pubs.acs.org/10.1021/acsomega.4c02869

Author Contributions

[▽]W.F. and Q.-Y.L. contributed equally. The manuscript was written through contributions of all authors. All authors have given approval to the final version of the manuscript.

Notes

The authors declare no competing financial interest.

■ ACKNOWLEDGMENTS

This work was supported by the National Natural Science Foundation of China (32171392), the Science and Technology Innovation Fund of Shenzhen (JCYJ20230807115818039), the Fundamental Research Funds for the Central Universities (2024CDJXY002), and high level discipline cultivation project of Shenzhen Polytechnic University.

■ REFERENCES

(1) Li, R. W.; Deng, Y.; Pham, H. N.; Weiss, S.; Chen, M.; Smith, P. N. Riluzole protects against skeletal muscle ischaemia-reperfusion injury in a porcine model. *Injury* **2020**, *51* (2), 178−184.

(2) Defraigne, J. O.; Pincemail, J. Local and systemic consequences of severe ischemia and reperfusion of the skeletal muscle. Physiopathology and prevention. *Acta Chir. Belg.* **1998**, *98* (4), 176−186.

(3) Blaisdell, F. W. The pathophysiology of skeletal muscle ischemia and the reperfusion syndrome: a review. *Cardiovasc. Surg.* **2002**, *10* (6), 620−630.

(4) Merchant, S. H.; Gurule, D. M.; Larson, R. S. Amelioration of ischemia-reperfusion injury with cyclic peptide blockade of ICAM-1. *Am. J. Physiol. Heart Circ. Physiol.* **2003**, *284* (4), H1260−H1268.

(5) Korthuis, R. J.; Granger, D. N.; Townsley, M. I.; Taylor, A. E. The role of oxygen-derived free-radicals in ischemia-induced increases in canine skeletal-muscle vascular-permeability. *Circ. Res.* **1985**, *57* (4), 599−609.

(6) Ekinci, Ş.; Kaldirim, Ü.; Akyildiz, F.; Bilgic, S.; Koca, K.; Poyrazoglu, Y.; Uysal, O. S.; Turgut, H.; Turkkan, S.; Ersen, Ö.; Topal, T.; et al. Effects of hypothermia on skeletal ischemia reperfusion injury in rats. *Open Med.* **2015**, *10* (1), 194−200.

(7) Takhtfooladi, M. A.; Shahzamani, M.; Takhtfooladi, H. A.; Moayer, F.; Allahverdi, A. Effects of light-emitting diode (LED) therapy on skeletal muscle ischemia reperfusion in rats. *Lasers Med. Sci.* **2015**, *30* (1), 311−316.

(8) Corrick, R. M.; Tu, H.; Zhang, D.; Barksdale, A. N.; Muelleman, R. L.; Wadman, M. C.; Li, Y.-L. Dexamethasone Protects Against Tourniquet-Induced Acute Ischemia-Reperfusion Injury in Mouse Hindlimb. *Front. Physiol.* **2018**, *9*, 244.

(9) Ergun, Y.; Kurutas, E. B.; Atalay, F.; Alic, T. Effects of silibinin and ethanol on skeletal muscle ischemia-reperfusion injury. *Acta Cir. Bras.* **2013**, *28* (3), 179−184.

(10) Huang, T.; Wang, W.; Tu, C.; Yang, Z.; Bramwell, D.; Sun, X. Hydrogen-rich saline attenuates ischemia-reperfusion injury in skeletal muscle. *J. Surg. Res.* **2015**, *194* (2), 471−480.

(11) Li, J.; Kataoka, K. Chemo-physical Strategies to Advance the in Vivo Functionality of Targeted Nanomedicine: The Next Generation. *J. Am. Chem. Soc.* **2021**, *143* (2), 538−559.

(12) Huang, Y.; Ren, J.; Qu, X. Nanozymes: Classification, Catalytic Mechanisms, Activity Regulation, and Applications. *Chem. Rev.* **2019**, *119* (6), 4357−4412.

(13) Zong, Q.; Chen, H.; Zhao, Y.; Wang, J.; Wu, J. Bioactive carbon dots for tissue engineering applications. *Smart Mater. Med.* **2024**, *5* (1), 1−14.

(14) Long, W.-J.; Yu, Y.; He, C. A novel and promising engineering application of carbon dots: Enhancing the chloride binding performance of cement. *Chin. Chem. Lett.* **2024**, *35* (6), 108943.

(15) He, H.; Du, L.; Xue, H.; An, Y.; Zeng, K.; Huang, H.; He, Y.; Zhang, C.; Wu, J.; Shuai, X. Triple Tumor Microenvironment-Responsive Ferroptosis Pathways Induced by Manganese-Based Imageable Nanoenzymes for Enhanced Breast Cancer Theranostics. *Small Methods* **2023**, *7* (7), 2300230.

(16) Liu, C.; Xiao, G.; Yang, M.; Zou, B.; Zhang, Z.-L.; Pang, D.-W. Mechanofluorochromic Carbon Nanodots: Controllable Pressure-Triggered Blue and Red Shifted Photoluminescence. *Angew. Chem., Int. Ed.* **2018**, *57* (7), 1893−1897.

(17) Liu, C.; Bao, L.; Tang, B.; Zhao, J.-Y.; Zhang, Z.-L.; Xiong, L.-H.; Hu, J.; Wu, L.-L.; Pang, D.-W. Fluorescence-Converging Carbon Nanodots-Hybridized Silica Nanosphere. *Small* **2016**, *12* (34), 4702−4706.

(18) Sun, H.; Zhao, A.; Gao, N.; Li, K.; Ren, J.; Qu, X. Deciphering a nanocarbon-based artificial peroxidase: chemical identification of the catalytically active and substrate-binding sites on graphene quantum dots. *Angew. Chem., Int. Ed.* **2015**, *54* (24), 7176−7180.

(19) Song, Y.; Qu, K.; Zhao, C.; Ren, J.; Qu, X. Graphene oxide: intrinsic peroxidase catalytic activity and its application to glucose detection. *Adv. Mater.* **2010**, *22* (19), 2206−2210.

(20) Gao, W.; He, J.; Chen, L.; Meng, X.; Ma, Y.; Cheng, L.; Tu, K.; Gao, X.; Liu, C.; Zhang, M.; et al. Deciphering the catalytic mechanism of superoxide dismutase activity of carbon dot nanozyme. *Nat. Commun.* **2023**, *14* (1), 160.

(21) Liu, C.; Fan, W.; Cheng, W.-X.; Gu, Y.; Chen, Y.; Zhou, W.; Yu, X.-F.; Chen, M.; Zhu, M.; Fan, K.; Luo, Q.-Y. Red Emissive Carbon Dot Superoxide Dismutase Nanozyme for Bioimaging and Ameliorating Acute Lung Injury. *Adv. Funct. Mater.* **2023**, *33* (19), 2213856.

(22) Ma, Y.; Zhao, J.; Cheng, L.; Li, C.; Yan, X.; Deng, Z.; Zhang, Y.; Liang, J.; Liu, C.; Zhang, M. Versatile carbon dots with superoxide dismutase-like nanozyme activity and red fluorescence for inflammatory bowel disease therapeutics. *Carbon* **2023**, *204*, 526−537.

(23) Ma, Y.; Gao, W.; Zhang, Y.; Yang, M.; Yan, X.; Zhang, Y.; Li, G.; Liu, C.; Xu, C.; Zhang, M. Biomimetic MOF Nanoparticles Delivery of C-Dot Nanozyme and CRISPR/Cas9 System for Site-Specific Treatment of Ulcerative Colitis. *ACS Appl. Mater. Interfaces* **2022**, *14* (5), 6358−6369.

(24) Zhang, Y.; Gao, W.; Ma, Y.; Cheng, L.; Zhang, L.; Liu, Q.; Chen, J.; Zhao, Y.; Tu, K.; Zhang, M.; et al. Integrating Pt nanoparticles with carbon nanodots to achieve robust cascade superoxide dismutase-catalase nanozyme for antioxidant therapy. *Nano Today* **2023**, *49*, 101768.

(25) Xu, Z.; Liu, G.; Zheng, L.; Wu, J. A polyphenol-modified chitosan hybrid hydrogel with enhanced antimicrobial and antioxidant activities for rapid healing of diabetic wounds. *Nano Res.* **2023**, *16* (1), 905−916.

(26) Fang, Y.; Nie, T.; Li, G.; Wang, L.; Du, J.; Wu, J. Multifunctional antibiotic hydrogel doped with antioxidative

lycopene-based liposome for accelerative diabetic wound healing. *J. Chem. Eng.* **2024**, *480*, 147930.
(27) Walker, P. M. Ischemia/Reperfusion Injury in Skeletal Muscle. *Ann. Vasc. Surg.* **1991**, *5* (4), 399−402.
(28) Gillani, S.; Cao, J.; Suzuki, T.; Hak, D. J. The effect of ischemia reperfusion injury on skeletal muscle. *Injury-Int. J. Care Inj.* **2012**, *43* (6), 670−675.
(29) Pan, L.; Sun, S.; Zhang, L.; Jiang, K.; Lin, H. Near-infrared emissive carbon dots for two-photon fluorescence bioimaging. *Nanoscale* **2016**, *8* (39), 17350−17356.
(30) Li, H. M.; Zhang, Q. Y.; Luo, X. T.; Yao, Z. H.; Qu, Y. Q.; Wang, E. R.; Jiang, B. B.; Qiu, Z. P.; Li, C.; Xu, Z. Q. Intrinsic dual emissive carbon dots for ratiometric sensing of acetylcholinesterase fluctuation induced by organophosphorus pesticide intoxication. *Sens. Actuators, B* **2022**, *373*, 132590.
(31) Zhang, S.; Xiao, C.; He, H.; Xu, Z.; Wang, B.; Chen, X.; Li, C.; Jiang, B.; Liu, Y. The adsorption behaviour of carbon nanodots modulated by cellular membrane potential. *Environ. Sci.: Nano* **2020**, *7* (3), 880−890.
(32) Lakowicz, J. R. *Principles of Fluorescence Spectroscopy*; Springer Science+Business Media, 2006.
(33) Wen, P.; Ke, W.; Dirisala, A.; Toh, K.; Tanaka, M.; Li, J. Stealth and pseudo-stealth nanocarriers. *Adv. Drug Delivery Rev.* **2023**, *198*, 114895.
(34) Kobayashi, A.; Kang, M. I.; Okawa, H.; Ohtsuji, M.; Zenke, Y.; Chiba, T.; Igarashi, K.; Yamamoto, M. Oxidative stress sensor Keap1 functions as an adaptor for Cul3-based E3 ligase to regulate proteasomal degradation of Nrf2. *Mol. Cell. Biol.* **2004**, *24* (16), 7130−7139.
(35) Mills, E. L.; Ryan, D. G.; Prag, H. A.; Dikovskaya, D.; Menon, D.; Zaslona, Z.; Jedrychowski, M. P.; Costa, A. S. H.; Higgins, M.; Hams, E.; et al. Itaconate is an anti-inflammatory metabolite that activates Nrf2 via alkylation of KEAP1. *Nature* **2018**, *556* (7699), 113−117.
(36) Barnig, C.; Lutzweiler, G.; Giannini, M.; Lejay, A.; Charles, A.-L.; Meyer, A.; Geny, B. Resolution of Inflammation after Skeletal Muscle Ischemia−Reperfusion Injury: A Focus on the Lipid Mediators Lipoxins, Resolvins, Protectins and Maresins. *Antioxidants* **2022**, *11* (6), 1213.
(37) Kim, S. F.; Huri, D. A.; Snyder, S. H. Inducible nitric oxide synthase binds, S-nitrosylates, and activates cyclooxygenase-2. *Science* **2005**, *310* (5756), 1966−1970.

https://doi.org/10.1021/acsomega.4c02869
ACS Omega 2024, 9, 28666−28675